Enhancement of Thermal and Optical Properties in ZnO-Doped POE/PCM($C_{25}H_{52}$) Composites

L. Maifi[a,b,*], A. Ayadi[c], O. Hioual[b,d], Z. Mezine[a], S. Taleb Hacine[b,e], K. Agroui[a] and A. Chari[b]

[a] *Research Research Center on Semiconductor Technology for Energetic, TESE-CRTSE, 2 BD, Frantz Fanon, 7 Merveilles, POB 140, Algiers, Algeria*
[b] *Laboratory of Thermodynamics and Surface Treatment in Materials, Department of Physics, University of Constantine 1, Frères Mentouri, Constantine, Algeria*
[c] *Laboratory of Microstructure and Defects in Materials, Department of Physics, University of Constantine 1, Frères Mentouri, Constantine, Algeria*
[d] *Computer Science Department, Abbes Laghrour Khenchela University, 40004, Khenchela, Algeria*
[e] *Faculty of Medicine, University of Batna 2, 05078, Batna, Algeria*

Received: 25.07.2025 & Accepted: 03.12.2025

Doi: 10.12693/APhysPolA.149.54 *e-mail: maifi.lyes@crtse.dz

This study investigates the enhancement of the thermal, structural, and optical properties of elastomeric polyolefin (POE)/phase change material (PCM($C_{25}H_{52}$)) composite polymers through the incorporation of zinc oxide (ZnO) nanoparticles, targeting applications in thermal energy storage, photovoltaics, and encapsulation. Composites were prepared with varying ZnO doping levels (0%, 10%, and 30%) and characterized using differential scanning calorimetry, thermogravimetric analysis, X-ray diffraction, scanning electron microscopy, Fourier transform infrared spectroscopy, and photoluminescence spectroscopy. The results demonstrate that the addition of ZnO nanoparticles significantly improves thermal stability, energy storage capacity, and heat transfer efficiency. The 30% ZnO-doped composite exhibited the highest melting temperature (90.5°C), no mass loss up to 180°C, and the greatest thermal conductivity, making it a promising candidate for thermal energy storage and encapsulation. X-ray diffraction analysis confirmed the successful incorporation of ZnO nanoparticles and an increase in crystallinity with doping, while photoluminescence spectra revealed enhanced optical properties due to defect passivation. The POE/PCM($C_{25}H_{52}$) matrix provides a stable environment that preserves the intrinsic properties of ZnO nanoparticles, enabling their effective integration into the composite. These findings highlight the potential of ZnO-doped POE/PCM($C_{25}H_{52}$) composites for advanced applications in thermal energy storage, heat management, optoelectronics, and encapsulation — particularly in photovoltaic systems, where uniform dispersion of ZnO nanoparticles can enhance light absorption, charge transport, and device durability.

topics: polymer composites, ZnO nanoparticles, phase change materials (PCM($C_{25}H_{52}$)), thermal conductivity

1. Introduction

As global energy demands rise, the development of efficient and sustainable thermal energy storage (TES) systems has become increasingly critical. Latent heat thermal energy storage (LHTES) using phase change materials (PCMs) offers high energy density and operational efficiency due to the process of absorbing and releasing heat at nearly constant temperatures during phase transitions [1–3]. Paraffin-based PCMs, in particular, are attractive due to their chemical inertness, thermal reliability, and affordability [4–6]. However, their inherent low thermal conductivity and leakage during melting limit their standalone application in practical systems [7–9]. To address these drawbacks, researchers have focused on form-stable composite PCMs, which incorporate PCMs into supporting matrices. These include: polyethylene, poly(methyl methacrylate) (commonly abbreviated as PMMA), and other polymers [10–12]. These matrices enhance structural stability and prevent leakage. For example, Li et al. [10] developed a paraffin/high-density polyethylene/wood flour composite with improved thermal storage stability, while Alkan and Sari [11] demonstrated that PMMA-fatty acid blends exhibited reliable latent heat storage performance.

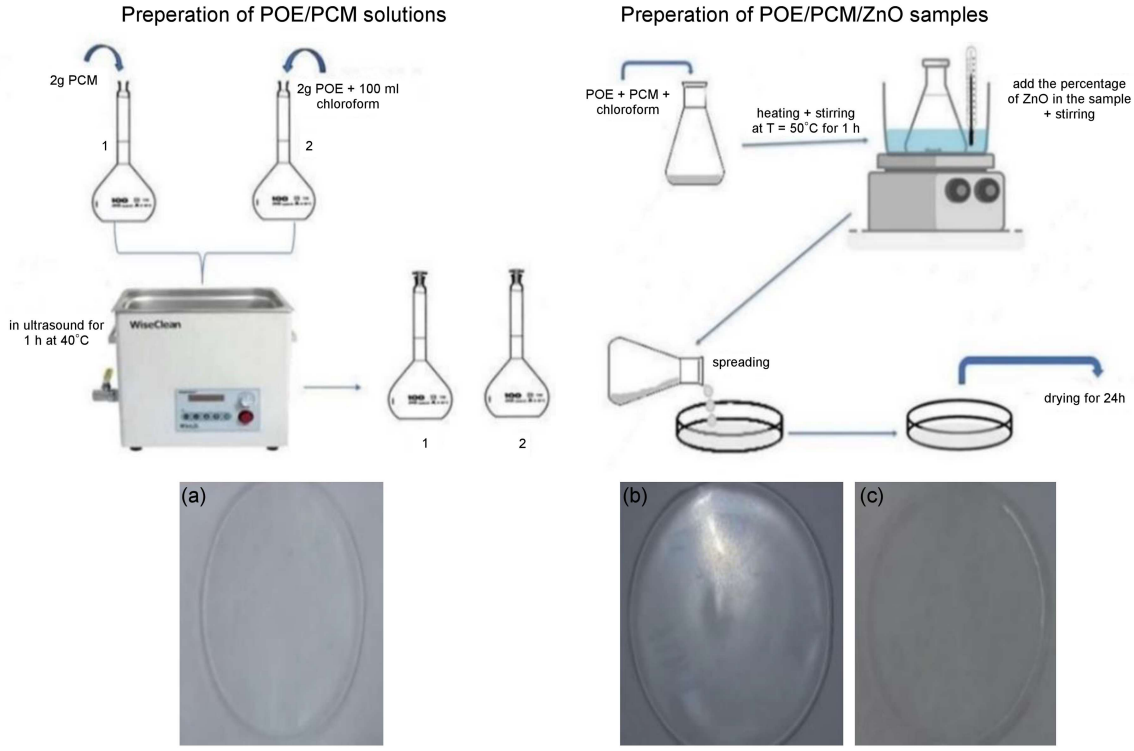

Fig. 1. Schematic representation of POE/PCM($C_{25}H_{52}$) composite polymer and ZnO-doped POE/PCM($C_{25}H_{52}$) preparation: (a) pristine POE/PCM($C_{25}H_{52}$), (b) POE/PCM($C_{25}H_{52}$)-10% at. ZnO, and (c) POE/PCM($C_{25}H_{52}$)-30% at. ZnO.

Recent studies have shown that polymer matrices not only prevent leakage but can also improve shape stability and reusability [12, 13].

Nanoparticle-enhanced PCMs have emerged as a promising solution for improving thermal conductivity and overall performance. Metal oxide nanoparticles such as ZnO, TiO_2, and Al_2O_3 have been incorporated into PCMs to improve both heat transfer and structural integrity [7, 14, 15]. Wang et al. [15] reported significant thermal enhancement of paraffin wax upon doping with TiO_2 nanoparticles. Similarly, polymer-based nanocomposites with metal oxides such as ZnO exhibit improved thermal stability, photostability, and optical response, which are essential in photovoltaic and optoelectronic applications [16–18]. In particular, ZnO has shown great potential for enhancing the thermal conductivity and ultraviolet (UV) blocking capacity of polymer composites [19–21]. Additionally, recent advances in encapsulation technologies such as spray drying, microencapsulation, and solvent casting have facilitated better integration and dispersion of PCMs within polymer matrices [13, 22], improving long-term durability and phase stability in repeated heating–cooling cycles [9, 23–27]. Our objective is to study the durability of the POE/PCM($C_{25}H_{52}$) composite for cooling photovoltaic panels and optimizing their optical and thermal efficiency. Our study focuses on preventing the transformation of PCM($C_{25}H_{52}$) into a liquid state by using POE polymer as a structural support and encapsulant due to its adhesive and transparent properties. Specifically, we investigate the characteristics of both pure and ZnO-doped POE/PCM($C_{25}H_{52}$) composites. We focus on the effect of ZnO doping on the thermal conductivity, optical, and thermal stability of the composite material.

2. Experimental section

The zinc oxide (ZnO) nanoparticles were first synthesized via a sol-gel method following the procedure established in our previous work, Benmammar et al. [28], which confirmed the optimal properties of ZnO. Zinc acetate dihydrate (20 g) was dissolved in 100 mL of deionized water under constant magnetic stirring at 25°C for 30 min, while a separate solution of citric acid dihydrate (2 g) in 200 mL of absolute ethanol was prepared. These solutions were then gradually combined, yielding a stable sol that was aged at 80°C for 24 h to form a gel. Subsequent calcination at 450°C for 2 h (at a heating rate of 5°C/min) produced a white crystallized ZnO nanopowder. For the polymer composite preparation, equimass quantities (2 g each) of phase change material (PCM($C_{25}H_{52}$)) and polyolefin elastomer

(POE) were separately dissolved in chloroform using ultrasonic assistance (40 kHz, 40°C, 1 h) to ensure complete dissolution. The solutions were combined and magnetically stirred (500 rpm) at 55°C while incorporating the pre-synthesized ZnO nanoparticles at two doping levels (10% and 30%, equivalent to 1.15 wt% and 3.45 wt%, respectively), as shown in Table I. The homogeneous mixture was solution-cast into Petri dishes and dried under ambient conditions for 24 h to produce three distinct composite films: pristine POE/PCM($C_{25}H_{52}$), POE/PCM($C_{25}H_{52}$)-10% at. ZnO, and POE/PCM($C_{25}H_{52}$)-30% at. ZnO. The experimental procedure and resulting composite samples are presented in the panels of Fig. 1, where (a) shows pristine POE/PCM($C_{25}H_{52}$), (b) POE/PCM($C_{25}H_{52}$)-10% at. ZnO, and (c) POE/PCM($C_{25}H_{52}$)-30% at. ZnO; this demonstrates the homogeneous dispersion of ZnO nanoparticles within the polymer matrix.

The structural properties of synthesized samples were analyzed using X-ray diffraction (XRD; Bruker D8 ADVANCE diffractometer with Bragg–Brentano geometry). XRD patterns were collected across a 2θ range from 27° to 80° with a step size of 0.2°. Morphological characterization was performed using high-resolution scanning electron microscopy (SEM; JEOL JSM-7610FPlus). Optical properties were investigated through photoluminescence (PL) spectroscopy at room temperature using a fluorescence spectrophotometer (Agilent Cary Eclipse). Fourier-transform infrared (FTIR) spectroscopy was conducted with an Agilent Cary 680 spectrometer, covering the spectral range of 400–8000 cm^{-1} at a resolution of 0.1 cm^{-1}. Thermal properties, including phase change temperature, latent heat, and mass loss, were evaluated using simultaneous differential scanning calorimetry and thermogravimetric analysis (DSC/TGA; METTLER TOLEDO) under nitrogen atmosphere (50 mL/min flow rate) with a heating rate of 10°C/min.

3. Results and discussion

Figure 2 presents the XRD patterns of the POE/PCM($C_{25}H_{52}$) polymer composite, pure ZnO nanoparticles, and ZnO-doped POE/PCM($C_{25}H_{52}$) composites with two different ZnO concentrations (i.e., 10% and 30%). The XRD pattern of the POE/PCM($C_{25}H_{52}$) composite exhibits a broad halo, characteristic of the amorphous segments within the polymer matrix. In contrast, the pure ZnO nanoparticles display distinct diffraction peaks at 2θ = 31.6°, 34.4○, 36.2°, 47.5°, 56.6°, 62.76°, 66.4°, and 77.0°, corresponding to the crystallographic planes (100), (002), (101), (102), (110), (103), (200), and (201), respectively. By comparing these peaks with a reference database [29],

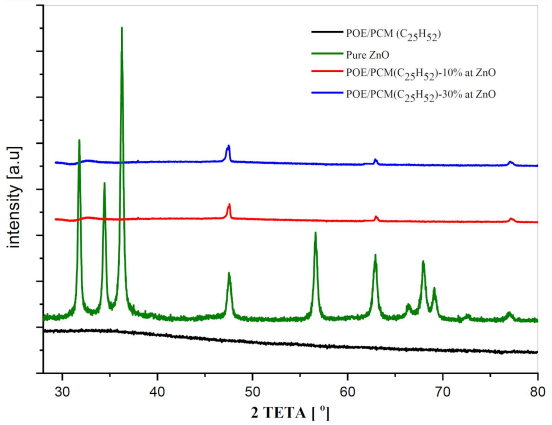

Fig. 2. X-ray diffraction patterns of POE/PCM($C_{25}H_{52}$) polymer composite, pure ZnO, POE/PCM($C_{25}H_{52}$)-10% at. ZnO, and POE/PCM($C_{25}H_{52}$)-30% at. ZnO.

the crystal structure of pure ZnO was identified as a polycrystalline phase consistent with the hexagonal wurtzite structure. In the ZnO-doped POE/PCM($C_{25}H_{52}$) composites (i.e., with 10% and 30% at. ZnO), the XRD patterns reveal significant changes. The most intense peaks of ZnO are notably reduced or absent, leaving a textured phase with three prominent peaks at 47°, 62°, and 77°. Instead of the initial sharp peaks, a low-intensity bump appears in the region corresponding to the first three peaks, suggesting a decrease in ZnO crystallinity within the POE/PCM($C_{25}H_{52}$) matrix. This observation indicates either a reduction in ZnO crystallization or a partial amorphization of ZnO due to its interaction with the polymer composite. Despite these changes, the presence of residual ZnO peaks confirms the successful incorporation of ZnO nanoparticles into the POE/PCM($C_{25}H_{52}$) composite. The XRD data were used to calculate the average crystallite size of ZnO nanoparticles embedded in a POE/PCM($C_{25}H_{52}$) polymer. The crystallite size D was calculated using Scherrer's formula [30]

$$D = \frac{0.9\lambda}{\beta \sin(\theta)}, \tag{1}$$

where λ is the wavelength of the incident Cu K_α radiation (λ = 1.5406 Å), θ is the diffraction angle, and β is the full width at half maximum (FWHM).

Table II presents the results regarding the average crystal size of ZnO nanoparticles embedded in a POE/PCM($C_{25}H_{52}$) polymer composite. The results indicate that the crystal size of the ZnO nanoparticles remains unchanged upon incorporation into the POE/PCM($C_{25}H_{52}$) matrix. This observation suggests that the polymer composite does not significantly alter the structural properties of the ZnO nanoparticles during the embedding process.

TABLE I

Mass quantities and atomic percent used in the experimental procedure.

Sample composition	Mass [g]	Mole number [mol]	Molar mass [g/mol]	Samples
POE	2	–	–	–
PCM($C_{25}H_{52}$)	2	0.0056	352	–
POE/PCM($C_{25}H_{52}$)	4	–	–	A
ZnO	0.46	0.0056	81.38	–
10% at. ZnO / 1.15 at.%	0.046	0.00056	–	B
30% at. ZnO / 3.45 at.%	0.138	0.00168	–	C

TABLE II

Full width at half maximum (FWHM) and average crystal size (D) of ZnO nanoparticles embedded in a POE/PCM($C_{25}H_{52}$) polymer composite.

Samples	2θ	(hkl) plane	FWHM	D [nm]
Pure ZnO	31.78	(100)	0.26462	19.48
	34.43	(002)	0.31385	
	36.26	(101)	0.33383	
	47.55	(102)	0.44456	
	62.90	(103)	0.48554	
	77.01	(202)	0.58862	
POE/PCM($C_{25}H_{52}$)-10% at. ZnO	47.51	(102)	0.28566	20.32
	63.00	(103)	0.30993	
	77.22	(202)	0.46138	
POE/PCM($C_{25}H_{52}$)-30% at. ZnO	47.42	(102)	0.35237	18.40
	62.93	(103)	0.30669	
	77.14	(202)	0.50617	

The stability of the ZnO crystal size in the POE/PCM($C_{25}H_{52}$) composite can be attributed to the nature of the interaction between the nanoparticles and the polymer matrix. The POE/PCM($C_{25}H_{52}$) composite likely provides a stable environment that preserves the intrinsic properties of the ZnO nanoparticles, including their crystal structure and size. This is an important finding, as it demonstrates that the functional properties of ZnO nanoparticles, such as their optical, electrical, or photocatalytic characteristics, may remain intact when integrated into the polymer composite [16, 31, 32]. The POE/PCM($C_{25}H_{52}$) polymer composite enables the dispersion of ZnO in the form of layers for photovoltaic applications.

The morphology of the synthesized ZnO powder is relatively uniform, characterized by spherical grains. The morphological analysis reveals particles that appear as agglomerated species with varying geometries. The average size of the ZnO particles is $\approx$ 32 nm, as shown in Fig. 3a. The distribution of the ZnO particles and their influence on the morphology of the POE/PCM($C_{25}H_{52}$) polymer composite were also investigated. As depicted in Fig. 3b, a homogeneous dispersion of the ZnO nanoparticles within the POE/PCM($C_{25}H_{52}$) polymer matrix was observed, with no significant signs of aggregation. This uniform distribution suggests effective integration of the nanoparticles into the polymer matrix, which is critical for optimizing the composite's properties.

The photoluminescence (PL) spectra obtained for the POE/PCM($C_{25}H_{52}$), POE/PCM($C_{25}H_{52}$)-10% at. ZnO, and POE/PCM($C_{25}H_{52}$)-30% at. ZnO polymer composites are shown in Fig. 4. The PL spectrum of the pure POE/PCM($C_{25}H_{52}$) composite reveals a broad emission band in the range of 430–600 nm, which is likely attributed to defect-related transitions or impurity states within the polymer matrix. These defects could arise from structural disorder, oxidation during processing, or the presence of additives in the material. The broad nature of the emission suggests a distribution of energy states rather than a single discrete transition, which is typical for amorphous or semi-crystalline polymers such as POE and PCM($C_{25}H_{52}$).

With the addition of ZnO nanoparticles, the PL spectra of the POE/PCM($C_{25}H_{52}$)-10% at. ZnO and POE/PCM($C_{25}H_{52}$)-30% at. ZnO composites show significant changes. Notably, the intensity of the PL emission increases with the concentration of ZnO, indicating that the ZnO nanoparticles play a key role in enhancing the radiative recombination processes in the composite.

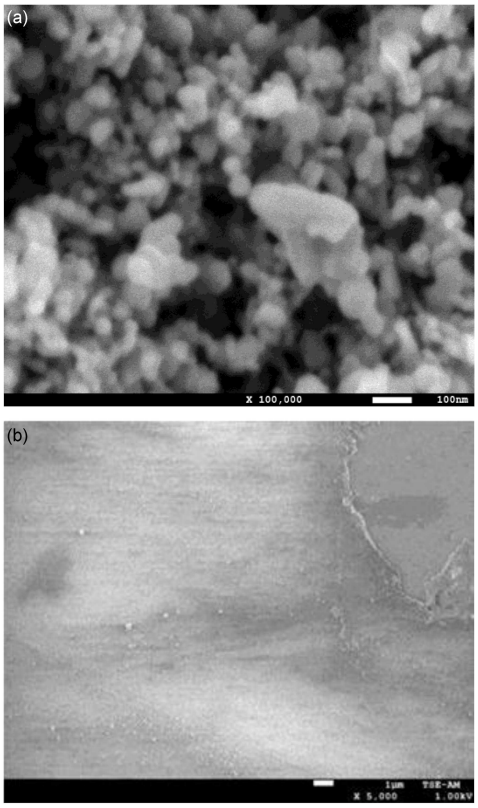

Fig. 3. SEM micrographs of (a) pure ZnO and (b) POE/PCM($C_{25}H_{52}$)-10% at. ZnO composite.

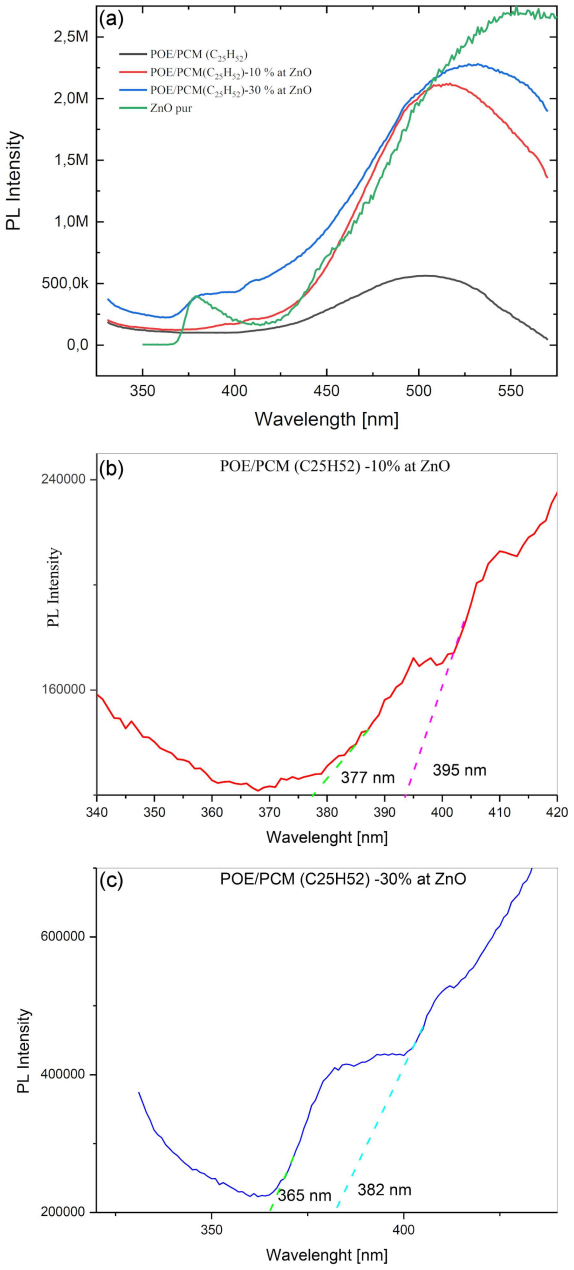

Fig. 4. (a) PL spectra of all considered composites: pure ZnO, POE/PCM($C_{25}H_{52}$), POE/PCM($C_{25}H_{52}$)-10% at. ZnO, and POE/PCM($C_{25}H_{52}$)-30% at. ZnO. (b, c) Bandgap properties shown for ZnO-doped POE/PCM composites, extracted from the spectra results in panel (a).

In the UV-visible range, the POE/PCM($C_{25}H_{52}$)-10% at. ZnO and POE/PCM($C_{25}H_{52}$)-30% at. ZnO composites exhibit two distinct shoulders in the range of 350–420 nm. The first shoulder, observed at 377 nm in POE/PCM($C_{25}H_{52}$)-10% at. ZnO and at 365 nm in POE/PCM($C_{25}H_{52}$)-30% at. ZnO, is likely due to defect states in ZnO, such as zinc interstitials (Zn_i) or oxygen vacancies (V_O). These defects create energy levels within the bandgap of ZnO and contribute to higher-energy emissions. However, as reported in [33], the embedding process can lead to a decrease in deep-level emission (defect-related emission) and an increase in near-band-edge (NBE) emission. This suggests that the polymer matrix may passivate some of the surface defects in ZnO, reducing the contribution of deep-level emission and enhancing the NBE emission.

The second shoulder, observed at higher wavelengths ($\sim$ 380–420 nm), corresponds to the near-band-edge (NBE) emission of ZnO, which arises from the radiative recombination of excitons (electron–hole pairs) in the ZnO nanoparticles [34]. This NBE emission is characteristic of ZnO. In our samples, it is observed at $\sim$ 395 nm ($\sim$ 3.14 eV) in POE/PCM($C_{25}H_{52}$)-10%at. ZnO and at $\sim$ 382 nm ($\sim$ 3.25 eV) in POE/PCM($C_{25}H_{52}$)-30% at. ZnO. The typical reference value for bulk ZnO is near $\sim$ 368 nm (3.36 eV). The shift in the emission wavelength can be attributed to quantum confinement effects or interactions with the polymer matrix, which modify the electronic structure of the ZnO nanoparticles.

The FTIR spectral analysis (Fig. 5) reveals distinct molecular interactions within the ZnO-doped POE/PCM($C_{25}H_{52}$) composites. A characteristic new peak appears around $\sim$ 500 cm^{-1} in the doped

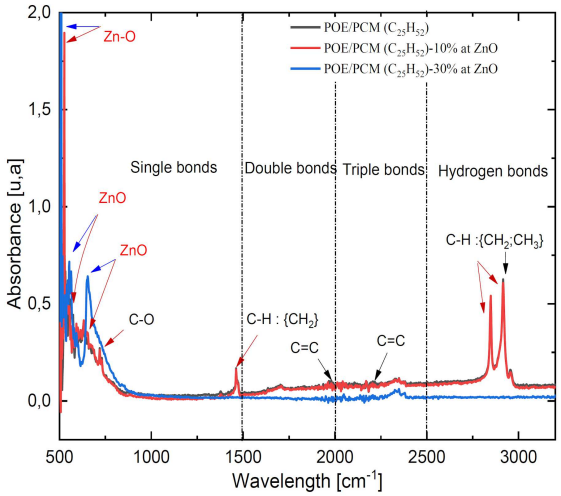

Fig. 5. FTIR spectra of pure and ZnO-doped POE/PCM($C_{25}H_{52}$) composites.

samples, which can be attributed to Zn–O stretching vibrations [15, 20], the intensity of which gradually increases from 10% to 30% ZnO loading, confirming the successful incorporation of ZnO nanoparticles. At higher ZnO concentrations, this Zn–O band exhibits slight broadening, which may be attributed to interfacial phonon scattering and localized interactions at the nanoparticle–polymer interface [1, 16, 35]. In the high-frequency region (3000–2500 cm^{-1}), characteristic C–H stretching vibrations of methyl (CH_3) and methylene (CH_2) groups are observed at $\approx$ 2870 and 2930 cm^{-1}, respectively [6, 12]. These bands progressively broaden and decrease in intensity with increasing ZnO content, suggesting enhanced interfacial bonding and restricted chain mobility in the polymer matrix [36]. In the mid-infrared range, absorption bands related to C $\equiv$ C (around 2200 cm^{-1}) and C = C (1600–1900 cm^{-1}) remain present, indicating that the fundamental carbon framework of POE is preserved. New absorption bands below 1100 cm^{-1}, corresponding to C–O and Zn–O interactions, become more defined with ZnO incorporation, suggesting potential covalent or coordination bonding between ZnO nanoparticles and oxygen-containing moieties in the PCM($C_{25}H_{52}$) or polymer backbone [18, 35]. Additionally, broad O–H stretching bands above 3400 cm^{-1} may indicate hydrogen bonding between hydroxyl groups on the ZnO surface and C–H bonds of the polymer [3, 7]. These observations align with reported interactions in polymer-based nanocomposites containing metal oxides [14, 36, 37]. Overall, the FTIR spectra confirm that ZnO nanoparticles not only integrate physically but also chemically with the POE/PCM($C_{25}H_{52}$) matrix through hydrogen bonding, coordination, and surface interactions, without compromising the integrity of the polymer structure.

The latent heat was evaluated through both experimental measurements and theoretical calculations. In Fig. 6a, we present the evolution of latent heat values versus ZnO doping concentration. It should be noted that there is a slight divergence between experimental and theoretical values. This discrepancy grows progressively with increasing ZnO content, which we attribute to the theoretical composite method employed [38].

The theoretical model allows us to calculate the doped material's latent heat L_{nm}, i.e.,

$$L_{nm} = L_m - 100\ \frac{\Delta H_{nm}}{\Delta H_m}\ \varphi. \tag{2}$$

The weight percentage of POE/PCM($C_{25}H_{52}$) in the composite is determined by

$$\text{POE/PCM } (C_{25}H_{52}) = 100\ \frac{\Delta H_{nm}}{\Delta H_m}, \tag{3}$$

where L_{nm} [J/g] represents the latent heat of pure POE/PCM, L_m [J/g] denotes the latent heat of the ZnO-doped ($C_{25}H_{52}$) composite, φ [%] is the ZnO doping concentration, ΔH_{nm} [J/g] is the enthalpy of pure POE/PCM($C_{25}H_{52}$), and ΔH_m [J/g] is the enthalpy of the ZnO-doped composite.

For higher mass percentages of nanoparticles in the POE/PCM($C_{25}H_{52}$) composite, the discrepancy between experimental and theoretical values becomes more pronounced. Similar variations have been reported by Sari et al. [39, 40], Sharma et al. [41], Chen et al. [42], and Wu et al. [43]. This observed deviation in latent heat values arises primarily from the theoretical composite method used for calculations and from morphological factors, including surface characteristics of the PCM($C_{25}H_{52}$), POE polymer structure, and nanoparticle dispersion efficiency within the PCMs matrix [39].

Solar cell encapsulation employs phase change materials (PCMs) designed for solid–liquid transitions at near-ambient temperatures (10–50°C above operational environments), leveraging latent heat accumulation at a defined phase transition temperature (T_f [°C]). These materials must be characterized for two critical properties, namely latent heat of fusion and melting temperature range [41]. Differential scanning calorimetry (DSC) precisely measures these parameters, using temperature gradient as a function of time (Fig. 6b), while thermogravimetric analysis (TGA) assesses thermal stability — a key for ensuring long-term performance under solar irradiance [41].

The DSC thermograms of POE/PCM($C_{25}H_{52}$) composite polymers and ZnO-doped composites at varying atomic fractions are presented in Fig. 6c. The melting point was identified as the endothermic peak maximum, while the glass transition temperature was determined through tangent analysis at the inflexion point of curve. Latent heat values were calculated by integrating the melting peak area following established protocols [6].

TABLE III

Thermal properties of PCM, POE/PCM($C_{25}H_{52}$), and POE/PCM($C_{25}H_{52}$) doped with 10% at. and 30% at. ZnO.

Sample	Experimental latent heat [J/g]	Calculated latent heat [J/g]	(POE/PCM) [%]	Melting point [°C]	Glass transition point [°C]	Phase change time [s]
PCM	154.56	–	–	55.30	46.83	38.4
POE/PCM	181.63	181.63	100	72.10	68.61	21.6
POE/PCM($C_{25}H_{52}$)-10 at.% ZnO	190.65	191.42	95.26	78.57	75.08	23.4
POE/PCM($C_{25}H_{52}$)-30 at.% ZnO	210.63	213.21	86.23	90.52	88.53	25.2

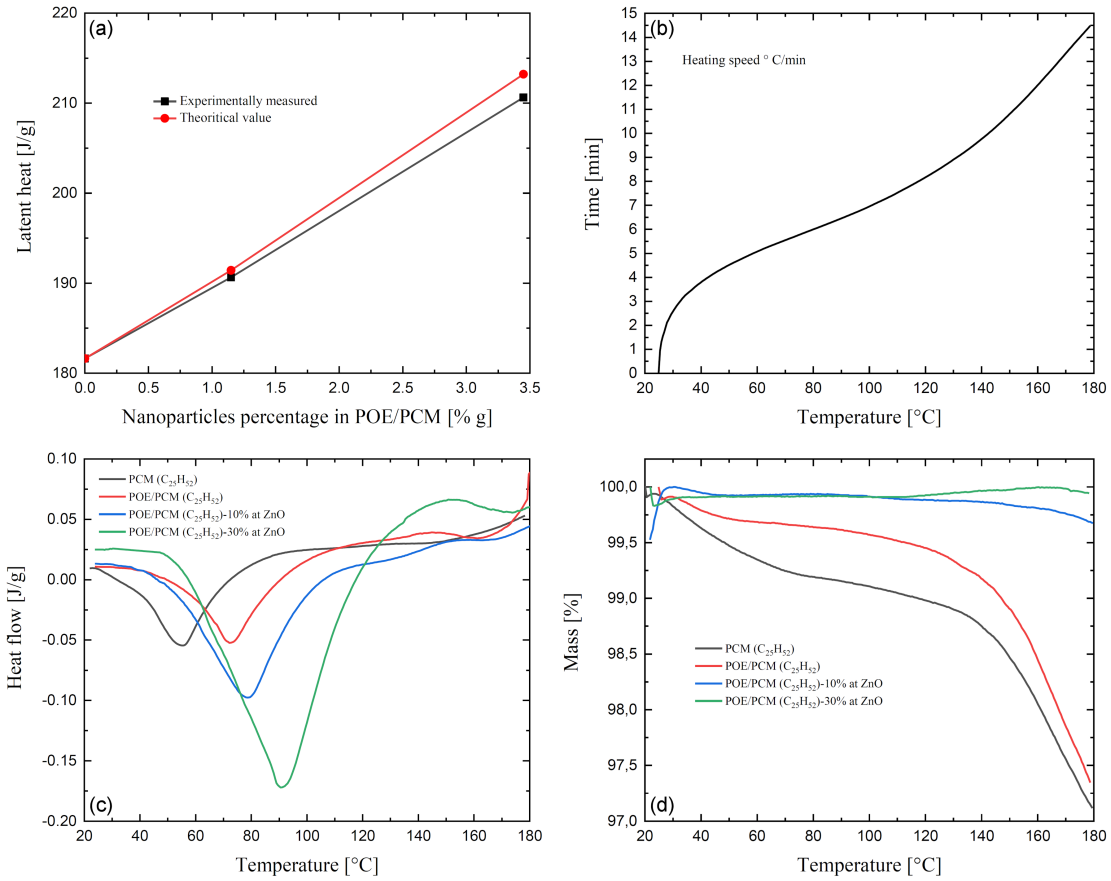

Fig. 6. Thermal characterization of the samples: (a) experimental and theoretical values of latent heat; (b) temperature gradient as a function of time used in DSC thermograms; (c) DSC thermograms of pure PCM, POE/PCM($C_{25}H_{52}$) composite polymers, and ZnO-doped composites, and (d) TGA curves of the same samples.

From the curves, the melting point and latent heat of POE/PCM($C_{25}H_{52}$) are presented in Table III. The weight percentage of POE/PCM($C_{25}H_{52}$) in the ZnO-doped POE/PCM($C_{25}H_{52}$) material was calculated using (3) [6], and the results are summarized in Table III. The data show that the melting points of PCM($C_{25}H_{52}$), POE/PCM($C_{25}H_{52}$), and ZnO-doped POE/PCM($C_{25}H_{52}$) differ, with a measured variation of 25%, confirming that the addition of ZnO nanoparticles modifies the melting behavior of both PCM($C_{25}H_{52}$) and POE/PCM($C_{25}H_{52}$). This observation is consistent with previous studies that showed that the addition of nanoparticles, including metal oxides, can influence phase transition temperatures and improve thermal response in PCM($C_{25}H_{52}$) composites [15, 37].

The latent heat increases steadily with the atomic percentage of ZnO nanoparticles (see Table III and Fig. 6). This trend is attributed to differences in the heat capacity of the constituents. The heat capacity of nanoparticles is higher than that of

both PCM($C_{25}H_{52}$) and the POE/PCM($C_{25}H_{52}$) composite. When ZnO nanoparticles are incorporated into POE/PCM, the resulting ZnO-doped POE/PCM($C_{25}H_{52}$) composite exhibits enhanced latent heat, which aligns with findings from other studies that reported improvements in energy storage capacity upon nanoparticle doping [6, 7, 15]. For example, Wang et al. [15] demonstrated that adding TiO_2 nanoparticles to paraffin significantly enhanced its thermal conductivity and latent heat, while Pielichowska and Pielichowski [7] reviewed similar enhancements with various nanomaterials. Sharma et al. [2] also observed that modifying PCM systems with nano-additives can enhance their latent heat and thermal performance.

The phase change duration of ZnO-doped POE/PCM($C_{25}H_{52}$) composites is longer than in their pure counterparts. Increasing the ZnO nanoparticle content in the POE/PCM($C_{25}H_{52}$) composite has two effects — it prolongs the phase change process and increases the latent heat.

The addition of more than 10% atomic nanoparticles is advisable because the melting temperature exceeds 80°C, reducing the risk of sedimentation when POE/PCM($C_{25}H_{52}$) is in the liquid state [38]. At 30% atomic nanoparticle loading, the maximum POE/PCM($C_{25}H_{52}$) loading reaches 86.23%, indicating a lower leakage risk compared to pure PCM($C_{25}H_{52}$). This is another advantage of ZnO-enhanced POE/PCM($C_{25}H_{52}$) over conventional PCM($C_{25}H_{52}$) [38]. However, exceeding 30% atomic nanoparticles is not recommended due to the increased sedimentation risk in the liquid phase [39]. Therefore, an optimal nanoparticle fraction should be maintained between 10 and 30%.

The transition temperature of pure POE is between 100 and 120°C. Therefore, it is not recommended to exceed a ZnO nanoparticle concentration of 30 at.%, where the melting temperature reaches 90.52°C — close to the POE transition range — which could pose a risk of ZnO leakage. It is thus necessary to ensure an optimal atomic fraction of nanoparticles between 10 and 30%.

POE serves as an effective support to prevent PCM($C_{25}H_{52}$) leakage during the solid–liquid transition and in the liquid phase, while maintaining the material's homogeneity and ensuring uniform dispersion of nanoparticles within the composite.

The impact of mass loss in Zn-doped POE/PCM($C_{25}H_{52}$) on thermal stability was investigated using thermogravimetric analysis (TGA). Figure 6d shows the TGA curves of POE/PCM($C_{25}H_{52}$) containing 10 to 30% at. ZnO after the initial heating cycles. While POE/PCM($C_{25}H_{52}$) liquefies at 50°C, its mass loss is negligible at temperatures below 120°C and is attributed to the evaporation of water in the material. It increases drastically at temperatures between 120 and 180°C, reaching 3% at 180°C. This mass loss can be interpreted as a complete breakdown of the POE and PCM($C_{25}H_{52}$) polymer chains into monomers starting at 120°C. For the 10% at. and 30% at. ZnO-doped POE/PCM($C_{25}H_{52}$) composites, there is practically no mass loss up to 180°C, which is beneficial for photovoltaic applications [2]. Furthermore, it appears that the more the atomic percentage of nanoparticles increases in the POE/PCM($C_{25}H_{52}$), the more the thermal stability of the material is improved.

The incorporated ZnO nanoparticles function as effective thermal stabilizers by raising the liquefaction onset temperature of the POE/PCM($C_{25}H_{52}$) matrix. This retardation effect stems from the nanoparticles' ability to restrict polymer chain mobility and provide thermal energy dissipation pathways. Crucially, the ZnO-doped POE/PCM($C_{25}H_{52}$) composites maintain structural integrity up to 180°C without detectable decomposition, as confirmed by thermogravimetric analysis. This thermal stability profile renders these materials particularly suitable for building-integrated solar energy storage systems and photovoltaic encapsulation applications [42]. The demonstrated temperature resistance, combined with the previously established phase change properties, positions these nanocomposites as promising candidates for renewable energy applications requiring durable thermal management solutions.

The phase change material (PCM), consisting of low-melting-point alkanes, forms an eutectic-like mixture with polyolefin elastomer (POE), resulting in a composite with depressed melting temperature relative to pure components. This binary system exhibits a reduced melting enthalpy compared to POE/PCM($C_{25}H_{52}$) mixtures of equivalent mass, as the constituent alkanes possess inherently higher latent heat capacity than the PCM($C_{25}H_{52}$) formulation. Notably, ZnO-doped composites (10 and 30 at.%) demonstrate enhanced thermal performance [43].

Based on the energy equation solution and the DSC data, numerous thermal conductivity calculation models have been developed to predict conductivity estimates for nanomaterials composed of highly regular elements, such as spherical nanoparticles. These models serve as valuable tools for understanding heat transfer in such materials.

An alternative expression for thermal conductivity calculation was introduced by Yu and Choi [44]. They proposed an advanced formulation that conceptualizes nanomaterials as a three-component system: (i) the base matrix material, (ii) solid nanoparticles, and (iii) an interfacial nanolayer acting as a thermal bridge between the constituent phases. This model takes into account the critical role of interfacial thermal resistance and particle-matrix interactions in determining the overall composite conductivity, i.e.,

$$K_m \frac{\partial^2 T}{\partial x^2} = \rho \frac{\partial Q}{\partial t}, \tag{4}$$

$$K_m = \frac{m_p}{e} \sum_{n=0}^{T} \frac{(Q_n - Q_{n-1})}{(T_n - T_{n-1})}, \quad (5)$$

$$\frac{K_{nm}}{K_m} = \frac{K_n + 2K_m + 2(K_m - K_n)(1-\beta)^3\varphi}{K_n + 2K_m - (K_m - K_n)(1-\beta)^3\varphi}, \quad (6)$$

where K_m [W/(m K)] represents the thermal conductivity of pure POE/PCM, K_{nm} [W/(m K)] denotes the thermal conductivity of the ZnO-doped POE/PCM composite, φ [%] is the ZnO doping concentration, ΔH_{nm} [J/g] is the enthalpy of pure POE/PCM and ΔH_m [J/g] is the enthalpy of the ZnO-doped composite, e [m] is the thickness, x [m] is the direction, m_p [g/s] is the mass flow rate, m [g] is the mass, ρ [kg/m^3] is the density, T [°C, K] is the temperature, t [s] is time, and c_p [J/(kg K)] is the specific heat.

Figure 7 presents the thermal conductivity values for PCM($C_{25}H_{52}$), POE/PCM($C_{25}H_{52}$), and their ZnO nanocomposites (10% and 30% at.). In the solid phase below the melting temperature, all samples exhibit relatively high thermal conductivity, ranging from 0.2 to 0.7 W/(m K). This enhanced conductive behavior stems from the material's dense, ordered crystalline structure that facilitates efficient phonon-mediated heat transfer. The phase transition region shows characteristic thermal conductivity fluctuations, where the onset of molecular disorganization during melting causes a temporary conductivity reduction. This occurs while the system maintains a theoretically constant temperature due to latent heat absorption.

Upon complete liquefaction, the thermal conductivity decreases significantly to ≈ 0.1 W/(m K), reflecting the transition to a disordered liquid state. While molecular mobility increases in the liquid phase, the breakdown of the regular crystalline structure and weaker intermolecular forces substantially reduce heat transfer efficiency. The nanocomposite systems demonstrate particular interest as the incorporated ZnO nanoparticles appear to mitigate this conductivity reduction, with the 30% ZnO formulation maintaining the highest conductivity values throughout all phase states.

The thermal conductivity increases significantly from 0.400 to 1.393 W/(m K) as the atomic percentage of ZnO rises from 0% to 30%, demonstrating a direct relationship between ZnO content and thermal performance enhancement. The addition of even small mass fractions of ZnO improves thermal conductivity in both solid and solid–liquid phases, with values increasing from 0.9456 to 1.393 W/(m K) when the ZnO doping level increases from 10% to 30%. This improvement is attributed to ZnO's ability to reconstruct efficient thermal pathways through Van der Waals interactions [45] while also providing phonon conduction channels within the composite [46]. Notably, the liquid phase exhibits only minimal conductivity gains [46, 47], as confirmed by prior studies

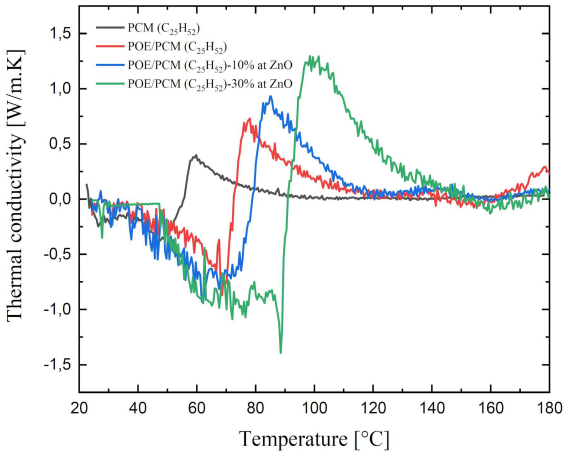

Fig. 7. Thermal conductivity of PCM($C_{25}H_{52}$), POE/PCM($C_{25}H_{52}$), and ZnO-doped POE/PCM($C_{25}H_{52}$) composites in solid and solid–liquid phases as a function of ZnO atomic percentage.

(Chen et al. [47]; Kim et al. [31]). The integration of high-thermal-conductivity ZnO nanoparticles into POE/PCM($C_{25}H_{52}$) polymers represents a major advancement for thermal energy management systems [48–50], particularly given that the base materials (POE polymer and paraffin PCM($C_{25}H_{52}$)) typically exhibit inherently low thermal conductivity (below 0.2 W/(m K)). The substantial conductivity enhancement achieved through ZnO doping thus addresses a critical limitation in these materials while expanding their potential for practical thermal applications.

4. Conclusions

The samples of PCM($C_{25}H_{52}$), POE/PCM($C_{25}H_{52}$), and their ZnO nanocomposites (10% and 30% atomic) have been successfully prepared. The XRD and FTIR results confirm the successful incorporation of ZnO nanoparticles into the polymer matrix and reveal an increase in crystallinity with higher doping levels. Additionally, a homogeneous dispersion of the ZnO nanoparticles within the POE/PCM($C_{25}H_{52}$) polymer matrix was confirmed by SEM imaging. The PL spectra show improved optical properties, which can be attributed to the passivation of defect states in the ZnO nanoparticles. This opens up interesting application possibilities in the field of water depollution, gas detection, and optoelectronics.

This study demonstrates that the incorporation of ZnO nanoparticles significantly enhances the thermal, structural, and optical properties of POE/PCM($C_{25}H_{52}$) composites. The 30% ZnO-doped composite exhibits the highest melting temperature (90.52°C), negligible mass loss, and the

greatest thermal conductivity, making it a highly promising candidate for thermal energy storage applications.

The POE/PCM($C_{25}H_{52}$) composite provides a stable environment that preserves the intrinsic properties of the ZnO nanoparticles, such as their structural parameter (D) and optical and photocatalytic characteristics (E_g), even when integrated into the polymer matrix. This stability is crucial for maintaining the functional performance of the nanoparticles in applications such as photovoltaics, where the uniform dispersion of ZnO in the form of layers can enhance light absorption and charge transport.

These findings highlight the potential of nanoparticle-doped composites to improve the performance of phase change materials in a wide range of applications, including thermal energy storage, heat management, and optoelectronics. The 30% ZnO-doped composite, in particular, stands out as a versatile material with enhanced thermal stability and optical properties, making it suitable for advanced energy-related technologies.

Acknowledgments

We thank Dr. Aissa KEFFOUS, Director of the *Centre de Recherche en Technologie des Semi-Conducteurs pour l'Energétique (CRTSE)*, and the members of the MEEC (TESE3) research team for their continuous support and valuable collaboration throughout this work. We would like to dedicate this work especially to Mr. Chari Abdelhamid, in recognition of his scientific guidance and generous assistance. Although now retired, he remains intellectually close to us. He is a true scientific reference, who continues to share his knowledge and experience selflessly, a living scientific library who moves among us to inspire and support.

References

[1] A. Abhat, *Solar Energy* **30**, 313 (1983).

[2] A. Sharma, V.V. Tyagi, C.R. Chen, D. Buddhi, *Renew. Sustain. Energy Rev.* **13**, 318 (2009).

[3] S.M. Hasnain, *Energy Conv. Manag.* **39**, 1127 (1998).

[4] S. Himran, A. Suwono, G.A. Mansoori, *Energy Sources.* **16**, 117 (1994).

[5] M. Hadjieva, S.T. Kanev, J. Argirov, *Solar Energy Mater. Solar Cells* **27**, 181 (1992).

[6] A.K. Ansu, R.K. Sharma, F.Y. Hagos, D. Tripathi, V.V. Tyagi, *J. Therm. Anal. Calorime.* **143**, 1881 (2020).

[7] K. Pielichowska, K. Pielichowski, *Prog. Mater. Sci.* **65**, 67 (2014).

[8] C. Alkan, *Thermochim. Acta* **451**, 126 (2006).

[9] M. Akgün, O. Aydin, K. Kaygusuz, *Energy Conv. Manag.* **48**, 669 (2007).

[10] J. Li, P. Xue, W. Ding, J. Han, G. Sun, *Solar Energy Mater. Solar Cells* **93**, 1761 (2009).

[11] C. Alkan, A. Sari, *Solar Energy* **82**, 118 (2008).

[12] S. Harikrishnan, M. Deenadhayalan, S. Kalaiselvam, *Energy Conv. Manag.* **86**, 864 (2014).

[13] S. Nagar, S. Sreenivasa, *Polym. Eng. Sci.* **64**, 4341 (2O24).

[14] P. Miluski, D. Dorosz, J. Zmojda, M. Kochanowicz, J. Dorosz, *Acta Phys. Pol. A* **127**, 730 (2015).

[15] J. Wang, H. Xie, Z. Guo, L. Guan, Y. Li, *Appl. Therm. Eng.* **73**, 1541 (2014).

[16] M. Bredács, C. Barretta, L.F. Castillon, A. Frank, G. Oreski, G. Pinter, S. Gergely, *Polym. Test.* **99**, 107406 (2021).

[17] M.R. Rodríguez, I. Sierra, A. Pérez Parada, L. Fornaro, *Environ. Sci. Pollut. Res.* **25**, 16767 (2018).

[18] S. Park, Y. Lee, Y.S. Kim, H.M. Lee, J.H. Kim, I.W. Cheong, W.G. Koh, *Colloid. Surf. A Physicochem. Eng. Asp.* **450**, 46 (2014).

[19] M. Lyes, K. Tahar, H. Ouided, C. Hamid, *Int. J. Multiphys.* **12**, 147 (2018).

[20] H. Bitter, S. Lackner, *Chem. Eng. J.* **423**, 129941 (2021).

[21] X. Jiang, R. Luo, F. Peng, Y. Fang, T. Akiyama, S. Wang, *Appl. Energy* **137**, 731 (2015).

[22] A. Gharssallaoui, G. Roudaut, O. Chambin, A. Voilley, R. Saurel, *Food Res. Int.* **40**, 1109 (2007).

[23] A. Kumar, K.M. Gangawane, in: *Materials for Boosting Energy Storage. Volume 3: Advances in Sustainable Energy Technologies*, American Chemical Society, 2024 ch. 13, p. 309.

[24] M.M. Farid, A.M. Khudhair, S.A.K. Razack, S. Al-Hallaj, *Energy Conv. Manag.* **45**, 1597 (2004).

[25] M. Świętek, W. Tokarz, J. Tarasiuk, S. Wroński, M. Błażewicz, *Acta Phys. Pol. A* **125**, 891 (2014).

[26] S.H. Mohamed, F.M. El-Hossary, G.A. Gamal, M.M. Kahlid, *Acta Phys. Pol. A* **115**, 704 (2009).

[27] A. Budkowski, A. Bernasik, E. Moons, M. Lekka, J. Zemla, J. Jaczewska, J. Haberko, J. Raczkowska, J. Rysz, K. Awsiuk, *Acta Phys. Pol. A* **115**, 435 (2009).

[28] F. Benmammar, A. Ayadi, L. Maifi, A. Chari, K. Agroui, *J. Sol-Gel Sci. Technol.* **112**, 870 (2024).

[29] S.C. Abrahams, J.L. Bernstein, *Acta Cryst. B* **25**, 1233 (1969).

[30] P. Scherrer, in: *Kolloidchemie Ein Lehrbuch*, Ed. R. Zsigmondy, P. Scherrer, Springer, Berlin 1918, p. 387 (in German).

[31] S. Park, Y. Lee, Y.S. Kim, H.M. Lee, J.H. Kim, I.W. Cheong, W.-G. Koh, *Colloid. Surf. A Physicochem. Eng. Asp.* **450**, 46 (2014).

[32] P. Yadav, V. Lahariya, P.P. Pandey, S. Behl, R. Raghav, *J. Mater. Sci. Mater. Electron.* **34**, 787 (2023).

[33] J.-P. Richters, T. Voss, L. Wischmeier, I. Rückmann, J. Gutowski, *Appl. Phys. Lett.* **92**, 011103 (2008).

[34] E. Cerrato, M.C. Paganini, E. Giamello, *J. Photochem. Photobiol. A Chem.* **397**, 112531 (2020).

[35] F. Bilgin, M. Arıcı, *Acta Phys. Pol. A* **132**, 1102 (2017).

[36] B. Zgardzinska, *Acta Phys. Pol. A* **127**, 1536 (2015).

[37] S. Wu, D. Zhu, X. Zhang, J. Huang, *Energy Fuels* **24**, 1894 (2010).

[38] R.K. Sharma, P. Ganesan, V.V. Tyagi, H.S.C. Metselaar, S.C. Sandaran, *Appl. Therm. Eng.* **99**, 1254 (2016).

[39] A. Sarı, A, Karaipekli, *Appl. Therm. Eng.* **27**, 1271 (2007).

[40] A. Sarı, A. Karaipekli, C. Alkan, *Chem. Eng. J.* **155**, 899 (2009).

[41] A. Sharma, P.K. Singh, E. Makki, J. Giri, T. Sathish, *Heliyon* **10**, e25800 (2024).

[42] H. Chen, B. Yang, H. Zhang, *J. Appl. Polym. Sci.* **77**, 928 (2000).

[43] S. Wu, D. Zhu, X. Zhang, J. Huang, *Energy Fuels.* **24**, 1894 (2003).

[44] W. Yu, S. Choi, *J. Nanopart. Res.* **5**, 167 (2003).

[45] A.R. Khantoul, M. Sebais, B. Rahal, B. Boudine, O. Halimi, *Acta Phys. Pol. A* **133**, 114 (2018).

[46] Y. Chen, Q. Zhang, X. Wen, H. Yin, J. Liu, *Solar Energy Mater. Solar Cells* **184**, 82 (2019).

[47] T.-H. Chen, Y.-C. Yeh, Y.-C. Liao, *ACS Appl. Mater. Interfaces* **10**, 24217 (2018).

[48] W. Wang, D. Li, J. Wu, L. Liu, Y. Sun, W. Ma, L. Ju, X. Lu, *Appl. Therm. Eng.* **258**, 124636 (2025).

[49] K.Y. Leong, M.R. Abdul Rahman, B.A. Gurunathan, *J. Energy Storage* **21**, 18 (2019).

[50] A. Gupta, R. Kumar, *Appl. Phys. Lett.* **91**, 223102 (2007).